Catalysis Science & Technology

Carboxylic Acid Ligand Substituent Impacts Hydrosilylation Activity of Platinum Single Atom Catalysts on Ceria

Journal:	*Catalysis Science & Technology*
Manuscript ID	CY-ART-06-2022-001017.R2
Article Type:	Paper
Date Submitted by the Author:	13-Oct-2022
Complete List of Authors:	Maciulis, Nicholas; Indiana University Wasim, Eman; Indiana University, Dept. of Chemistry Rezvani, Fereshteh; Indiana University Bloomington, Chemistry Pink, Maren; Indiana University Sterbinsky, George; Argonne National Laboratory Advanced Photon Source Caulton, Kenneth; Indiana University, Department of Chemistry Tait, Steven; Indiana University, Dept. of Chemistry

SCHOLARONE™
Manuscripts

Journal: Catalysis Science & Technology

Carboxylic Acid Ligand Substituent Impacts Hydrosilylation Activity of Platinum Single Atom Catalysts on Ceria

Nicholas A. Maciulis,[a] Eman Wasim,[a] Fereshteh Rezvani,[a] Maren Pink,[a] George E. Sterbinsky,[b] Kenneth G. Caulton,[a] and Steven L. Tait[a]

[a] Department of Chemistry, Indiana University, 800 E. Kirkwood Ave., Bloomington, Indiana 47405 (U. S. A.).

* E-mail: tait@indiana.edu, Tel.: +1-812-855-1302.

[b] Advanced Photon Source, Argonne National Laboratory, 9700 S. Cass Ave., Lemont, Illinois 60439 (U. S. A.).

Abstract

Current industrially employed hydrosilylation catalysts rely on homogeneous platinum catalysts which are not recovered after the reaction. To eliminate this issue, our group has been working to optimize recyclability of heterogeneous platinum single atom catalysts (SACs) on ceria via 1,10-phenanthroline-5,6-dione ligands (PDO), which incorporates mono (PDO-C) and dicarboxylic acid (PDO-C2) groups in the 2- and 9-position of PDO ligand to increase metal-surface interaction. DRIFTS results confirm carboxylic acid coordination to the terminal hydroxy groups of the ceria surface. New catalyst synthesis conditions wherein PDO was combined with the metal prior to exposure to the surface allow control of Pt oxidation state on the surface. The highest metal loading was observed for PDO and PDO-C, correlating with improved catalytic recyclability compared to the PDO-C2 ligand. It is proposed that the location of the carboxylic acid groups and the steric effects can explain the lower activity and metal loading for PDO-C2 ligands. Post-reaction XPS and DRIFTS spectra show the appearance of new Si and O species on the catalyst during the hydrosilylation reaction, indicating the silane reagent is depositing on the surface. The silane coverage and leaching of catalyst from the surface is the cause for the reduced catalytic activity.

1. Introduction

Hydrosilylation, the addition of silicon hydride bonds across unsaturated molecules (Scheme 1), has industrial applications in silicone-based materials[1-8] such as resins, adhesives, oils, lubricants, and coatings.[9-11] In 1957, Speier's catalyst H_2PtCl_6/^{i}PrOH[12] was employed until it was further improved in 1973 with Karstedt's platinum(0) complex containing a vinyl-siloxane ligand.[13, 14] Other metals have been explored but do not compare with the activity of platinum hydrosilylation catalysts.[15-23]

There is long-standing interest in developing heterogeneous catalysts for this reaction that would allow for more facile catalyst recovery, including work with heterogeneous single atom catalyst sites.[24, 25] Despite some reports stating that colloidal Pt also catalyzes hydrosilylation,[26-28] the dominant opinion is that Pt aggregation leads to deactivation.[9, 29, 30] Our prior work with Pt-ligand single-site catalyst systems also indicated that colloidal Pt present in those systems was not the main active species.[31] Thus, due to the high demand and value of platinum, efforts have been directed towards developing heterogeneous single atom catalysts (SAC)[32-34] that enable catalyst recovery.

Our research has focused on optimizing platinum hydrosilylation catalysts using redox active ligand platforms on oxide supports.[31] Metal oxides contain hydroxy sites that can stabilize species through hydrogen bonding or graft molecules onto the surface. Recently, the pretreatment of the ceria surface with arenes containing multiple carboxylic acid groups has demonstrated improved recyclability of platinum catalysts.[35]

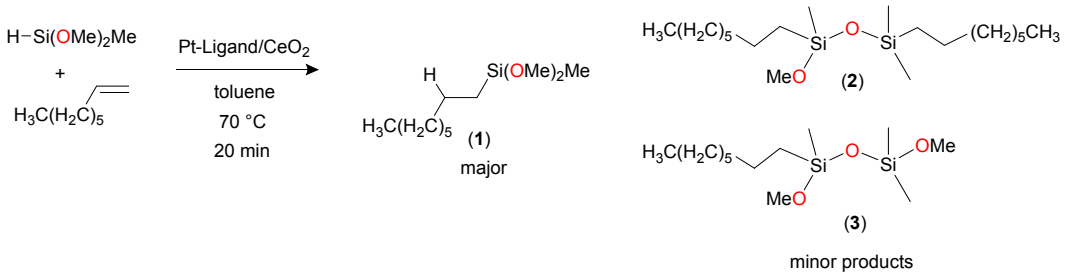

Scheme 1. Reaction conditions for testing hydrosilylation activity of ceria supported catalysts and major, desirable (1) and minor (2 and 3) products of the reaction.

In this paper, we report the syntheses of new ligands for ligand-coordinated supported catalysts incorporate carboxylic acid groups to increase ligand-surface interactions and metal-surface interactions in order to reduce leaching of metal during catalysis. Of the several ligands explored by our group, the 1,10-phenanthroline-5,6-dione (PDO) ligand gave the best reactivity, recyclability, and selectivity.[31, 35] The phenanthroline-4,4'dicarboxylic acid ligand (BPDCA) showed high metal loading but no activity.[36] Combining these characteristics, synthetic routes[37-39] were found to incorporate carboxylic acid groups into the PDO framework close to the nitrogens in order to increase metal surface interactions (Scheme 2).

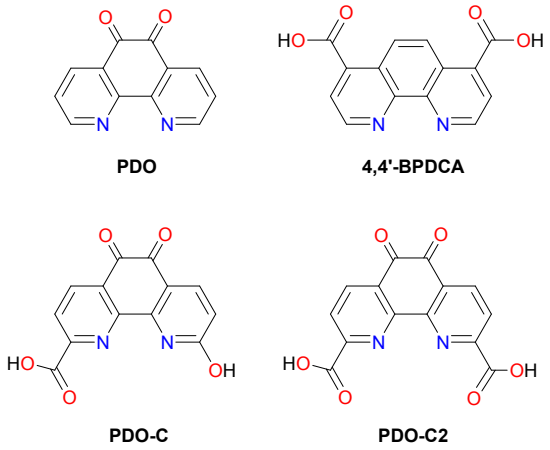

Scheme 2. Target ligands for anchoring platinum to surface: 1,10-phenanthroline-5,6-dione (PDO), 2,2'-bipyridine-5,5'-dicarboxylic acid (4,4'-BPDCA), 5,6,9-trioxo-5,6,9,10-tetrahydro-1,10-phenanthroline-2-carboxylic acid (PDO-C) and 5,6-dioxo-5,6-dihydro-1,10-phenanthroline-2,9-dicarboxylic acid (PDO-C2).

In this work, we report a detailed investigation of how the carboxylic acid groups incorporated into the PDO ligand impact recyclability of our ceria-supported platinum catalysts. Different impregnation methods were systematically explored to control oxidation state of Pt and improve Pt loading. Pt-Ligand complexes were studied on ceria supports, where ligand is either PDO, PDO functionalized asymmetrically with one carboxylic acid group (PDO-C), or PDO functionalized symmetrically with two carboxylic acid groups (PDO-C2, Scheme 2). The Pt SACs prepared show improved selectivity, recyclability, and lower platinum nanoparticle formation compared to previously published work.[31, 35] The discovery of silane buildup on the surface, in addition to metal leaching, was identified as a cause of recycle-induced decline in catalytic activity.

2. Experimental

2.1 General Experimental

Deuterated solvents were purchased from Cambridge Isotopes and were used as received. PDO-C2 was synthesized using literature procedures.[37-39] Neocuproine was purchased from AbovChem. Solvents, selenium dioxide, trimesic acid, 4-fluorobenzoic acid, KBr, Me_3SiCl, Me_2SiCl_2, and $PhSi(OMe)_3$ were purchased from Sigma Aldrich and used as received. $HSi(OMe)_2Me$ was purchased from TCI Chemicals. HNO_3 and H_2SO_4 was purchased from Macron. $PtCl_2(MeCN)_2$ was synthesized[40] from K_2PtCl_4 purchased from Strem Chemicals. PDO was purchased from AK scientific. Cerium(IV) oxide and 1-octene were purchased from Alfa Aesar.

XPS measurements were performed with a PHI Versaprobe II XP spectrometer using a monochromated Al X-ray source. A small amount of each powder sample was fixed onto a platen with double-sided tape. For CeO_2-supported samples, XPS were collected at Pt 4f, N 1s, C 1s, Cl 2p, Ce3d, O 1s, and Si 2p regions. A neutralizer was used to alleviate surface charging. The binding energy was corrected with C 1s peak (284.8 eV) for samples not supported on ceria, and Ce 3d5/2

main peak (882.0 eV) for CeO_2-supported samples. XPS data was processed using CasaXPS software.

DRIFTS spectra were collected in air using a Perkin Elmer Spectrum 100 FT-R fitted with a Pike Easi Diff – workhorse diffuse reflectance accessory.

Agilent 6890N GC and 5973 Inert MSD is a gas chromatograph with a quadrupole mass spectrometer using electron ionization with a 30 m 0.25 mm i.d. DB-5MS column to quantify anti-Markovnikov product using decane as an internal standard.

Samples were analyzed utilizing an Agilent 7700 ICP-MS within the Metal Isotopes Laboratory at Indiana University. Calibration standards for the elements of interest were prepared from commercial ICP-MS standards in dilute HCl, with concentrations ranging from 5 ppb to 1000 ppb. Each sample analysis consisted of five replicates, each with 100 sweeps, which were then averaged. Standards and blanks were run during the analytical session to ensure reproducibility. Blanks were always significantly below 1 ppb. Long-term precision for the instrument is within +/- 5%.

2.2 Ligand Synthesis

Synthesis of PDO-C

A 100 mL round bottom flask equipped with a stir bar was loaded with 0.275 g H_2PtCl_6 (0.671 mmol), 10 mL of glacial acetic acid, and 10 mL of deionized water. To this was added 0.200 g PDO-C2 (0.671 mmol) as a solid. A reflux condenser was attached, and the mixture heated at 90 °C for 24 hours during which the solution turned from orange solution to a reddish-orange color. Upon cooling to room temperature, a reddish-orange solid precipitated. The red mother liquor was decanted, and the resulting red-orange solid was washed with deionized water to give a red-orange solid (75 % yield), which was placed under vacuum. ^{1}H NMR (500 MHz, DMSO-d_6): δ (ppm) 13.49 (s, 1H), 12.77 (s, 1H), 8.57 (d, *J* = 8.0 Hz, 1H), 8.36 (d, *J* = 8.0 Hz, 1H), 8.02 (d, *J* = 9.5 Hz, 1H), 6.65 (d, *J* = 9.5 Hz, 1H) ; ^{13}C NMR (500 MHz, DMSO-d_6): δ (ppm) 176.1, 174.1, 163.8, 162.2, 148.7, 145.6, 144.8, 137.7, 137.3, 131.1, 126.4, 122.8, 114.7. FTIR (KBr, cm^{-1}): 1122, 1419, 1302, 1574, 1602, 1641, 1701, 1745, 2924, 3093, and 3512.

2.3 Catalyst Synthesis

Synthesis of Pt/CeO2

A 20 mL vial equipped with a stir bar was loaded with 0.010 g $PtCl_2(MeCN)_2$ (0.029 mmol) and 0.300 g CeO_2 in 20 mL of deionized water. The heterogeneous white solution was allowed to stir for 20 hours. The catalyst was centrifuged and washed three times with water then three times with acetonitrile until the washings ran clear. The white solid was placed under dynamic vacuum to remove volatiles. Based on ICP analysis, about 16.6 % of the Pt from the precursor slurry is loaded in the final catalyst.

Synthesis of Pt-PDO/CeO_2 using Method 1

A 20 mL vial equipped with a stir bar was loaded with 0.010 g PDO (0.048 mmol) and 0.300 g CeO_2 in 10 mL of deionized water. The heterogeneous, yellow solution was stirred for 1.5 hours. Subsequently, a slurry of 0.016 g $PtCl_2(MeCN)_2$ (0.048 mmol) in 10 mL of deionized water was added dropwise over a period of ten minutes and then stirred for 12 hours. The heterogeneous solution was centrifuged and washed 3 times with water and 3 times with acetonitrile until washings became colorless. Based on ICP analysis, about 4.35 % of the Pt from the precursor slurry is loaded in the final catalyst.

Synthesis of Pt-PDO-C/CeO_2 using Method 1

A 20 mL vial equipped with a stir bar was loaded with 0.010 g PDO-C (0.037 mmol) and 0.300 g CeO_2 in 10 mL of deionized water. The heterogeneous, orange solution was stirred for 1.5 hours. Subsequently, a slurry of 0.012 g $PtCl_2(MeCN)_2$ (0.037 mmol) in 10 mL of deionized water was added dropwise over a period of ten minutes and then stirred for 12 hours. The heterogeneous orange solution was centrifuged and washed 3 times with water and 3 times with acetonitrile until washings became colorless. The pale-orange solid was placed under vacuum. Based on ICP analysis, about 16.5 % of the Pt from the precursor slurry is loaded in the final catalyst.

Synthesis of Pt-PDO-C2/CeO_2 using Method 1

A 20 mL vial equipped with a stir bar was loaded with 0.010 g PDO-C2 (0.033 mmol) and 0.300 g CeO_2 in 10 mL of deionized water. The heterogeneous, white solution was stirred for 1.5 hours. Subsequently, a slurry of 0.011 g $PtCl_2(MeCN)_2$ (0.033 mmol) in 10 mL of deionized water was added dropwise over a period of ten minutes and then stirred for 12 hours. The heterogeneous solution was centrifuged and washed 3 times with water and 3 times with acetonitrile until washings became colorless. The off-white solid was placed under vacuum. Based on ICP analysis, about 1.01 % of the Pt from the precursor slurry is loaded in the final catalyst.

Synthesis of Pt-PDO/CeO_2 using Method 2

A 20 mL vial equipped with a stir bar was loaded with 0.010 g PDO (0.048 mmol), 0.016 g $PtCl_2(MeCN)_2$ (0.048 mmol), 15 mL of deionized water, and allowed to stir for 12 hours, during which time the solution turned faint blue in color. To this homogeneous solution, 0.300 g CeO_2 and 5 mL of deionized water were added and the resulting heterogeneous, blue solution was stirred for 12 hours. The heterogeneous solution was centrifuged and washed 3 times with water and 3 times with acetonitrile until washings became colorless. The solid was placed under vacuum to afford an off-white solid. Based on ICP analysis, about 18.4 % of the Pt from the precursor slurry is loaded in the final catalyst.

Synthesis of Pt-PDO-C/CeO_2 using Method 2

A 20 mL vial equipped with a stir bar was loaded with 0.010 g PDO-C (0.037 mmol), 0.012 g $PtCl_2(MeCN)_2$ (0.037 mmol), 8 mL of deionized water, and allowed to stir for 12 hours, during which time the solution turned orange in color. To this homogeneous solution, 0.300 g CeO_2 and 8 mL of deionized water were added and the resulting heterogeneous, orange-red solution was stirred for 12 hours. The heterogeneous solution was centrifuged and washed 3 times with water and 3 times with acetonitrile until washings became colorless. The solid was placed under

vacuum to afford a pale-orange solid. Based on ICP analysis, about 15.6 % of the Pt from the precursor slurry is loaded in the final catalyst.

Synthesis of Pt-PDO-C2/CeO_2 using Method 2

A 20 mL vial equipped with a stir bar was loaded with 0.010 g PDO-C2 (0.033 mmol), 0.011 g $PtCl_2(MeCN)_2$ (0.033 mmol), 8 mL of deionized water, and allowed to stir for 12 hours, during which time the solution turned white in color. To this homogeneous solution, 0.300 g CeO_2 and 8 mL of deionized water were added and the resulting heterogeneous, off-white solution was stirred for 12 hours. The heterogeneous solution was centrifuged and washed 3 times with water and 3 times with acetonitrile until washings became colorless. The solid was placed under vacuum to afford an off-white solid. Based on ICP analysis, about 5.84 % of the Pt from the precursor slurry is loaded in the final catalyst.

2.4 Binding carboxylic acids to prove binding to Ceria

Reaction of trimesic acid (TMA) + CeO_2 in water

A vial equipped with a stir bar was loaded with 0.300 g CeO_2 and 0.080 g TMA (0.38 mmol) and 20 mL of H_2O. The heterogeneous solution stirred for 12 hours and subsequently washed with water several times and then acetonitrile before drying under vacuum for 12 hours.

Reaction of 4-fluorobenzoic acid + CeO_2 in water

A vial equipped with a stir bar was loaded with 0.300 g CeO_2 and 0.100 g 4-fluorobenzoic acid (0.70 mmol) and 20 mL of H_2O. The heterogeneous solution stirred for 12 hours followed by washing with water several times then acetonitrile before drying under vacuum for 12 hours.

2.5 Hydrosilylation reaction

A pressure tube was loaded with 0.030 g of catalyst and 3 mL of toluene. The reaction mixture was allowed to stir at 70 °C for 10 minutes before addition of 0.337 g (0.47 mL) 1-octene (3.0 mmol) and 0.263 g $HSi(OMe)_2Me$ (2.5 mmol). The tube was sealed with a Teflon cap and heated for 20 minutes at 70 °C to prevent full conversion to compare yields between catalysts and batch cycles. At the end of the reaction, the flask was cooled by running cold water over the flask. The mixture then was centrifuged to isolate the solid from the mother liquor for reuse or post characterization. Dilution of 1 mL of reaction solution in a 25 mL volumetric flask with toluene allowed for GCMS analysis. The catalyst was centrifuged and washed three times with toluene between batch cycles.

2.6 Silylation of Ceria

Representative reaction of Me_3SiCl and Me_2SiCl_2 with CeO_2

A test tube equipped with a stir bar was loaded with 0.300 g CeO_2 and placed in a wide-mouth Schlenk flask. The flask was evacuate-refill cycled with argon several times. Then, 0.5 mL of Me_3SiCl or Me_2SiCl_2 were added and placed under static vacuum for 12 hours to stir the ceria under a silane atmosphere. Volatiles were removed under vacuum followed by rinsing the ceria 3 times with deionized water to remove HCl. The white solid was placed under vacuum to remove volatiles.

Representative reaction of $HSi(OMe)_2Me$ and $PhSi(OMe)_3$ with CeO_2

A pressure tube equipped with a stir bar was loaded with 0.300 g CeO_2 and 4 mL of toluene. To this was added 0.300 g $HSi(OMe)_2Me$ (2.85 mmol) and the reaction flask was heated at 70 °C for 2 hours. $PhSi(OMe)_3$ was heated for 12 hours. The samples were washed with toluene three times followed by drying under dynamic vacuum for 12 hours.

3. Results and Discussion

3.1 Ligand synthesis

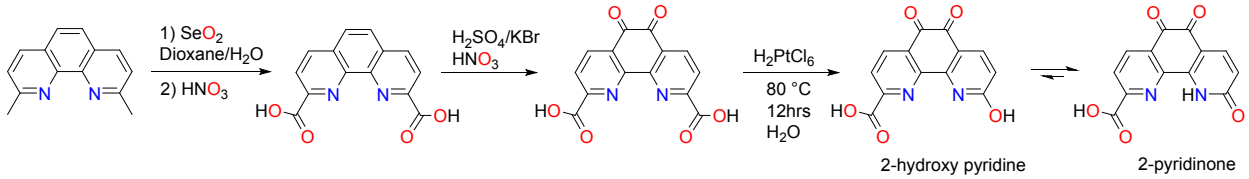

Scheme 3. Synthesis of PDO-C2 and PDO-C.

The PDO-C2 ligand was synthesized by successive oxidation of 2,9-dimethyl-1,10-phenanthroline (Scheme 3) following established procedures outlined in experimental section. The PDO-C2 undergoes oxidative decarboxylation[41, 42] to give the asymmetric PDO-C ligand shown in Scheme 3.

The ^1H NMR spectrum of PDO-C shows four doublets in the aromatic region (Fig. S2) and the ^{13}C NMR spectrum shows the presence of 13 signals indicating loss of C_{2v} symmetry (Fig. S3). X-ray diffraction data confirm spectral observations and mono decarboxylation of PDO-C2 (Fig. 1). X-ray diffraction data of the orange crystal obtained from a concentrated DMSO solution indicate that the structure contains 98% of PDO-C ligand and 2% of it as a platinum complex (Fig. 1 and S7, respectively). Hydrogen bonding between DMSO and ligand is indicated by dashed yellow lines [N1-H1n…O6, 1.90(2) Å, and O5-H5o…O6, 1.80(3) Å]. The hydrogen atoms involved in hydrogen bonding were found in the difference map and refined freely. For protonated N1, longer N-C bond lengths are observed [N1-C1 1.397(2) Å and N1-C12 1.355(2) Å] compared to N2-C10 and N2-C11 [1.335(2) Å and 1.334(2) Å, respectively]. Likewise, protonated O5 features a longer C-O distance compared to O4 [C13-O4 1.206(2) Å and C13-O5 1.321(2) Å].

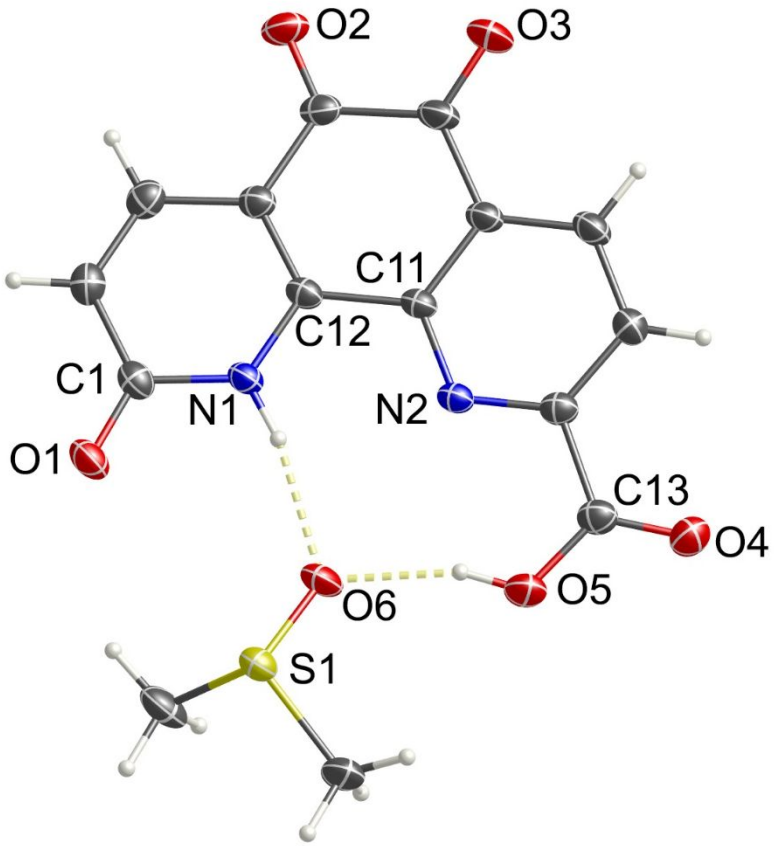

Fig. 1. Crystal structure of PDO-C·DMSO; relevant distances (Å) are as follows: N1-C12, 1.355(2); N1-C1, 1.397(2); C1-O1, 1.233(2); N2-C11, 1.334(2); N2-C10, 1.335(2); C13-O5, 1.321(2); C13-O4, 1.206(2); N1-O6, 2.790; and O5-O6, 2.628; yellow dashed lines indicate hydrogen bonds.

PDO-C can exist as two tautomers (Scheme 3), 2-pyridinone and 2-hydroxy pyridine, the former being favored in solution and solid state. Coordination to a metal likely will favor the latter yielding a metal complex with an anchor and a proton responsive site in the secondary coordination sphere that could impact selectivity.

3.2 Catalyst Synthesis

PDO-C and PDO-C2 are now compared to PDO to study how the number of anchor groups impact catalyst impregnation and leaching. Previous synthesis of SACs used H_2PtCl_6 as the metal precursor with 3 equivalents of ligand in protic solvents.[31, 35] Since XPS showed that Pt(II) was the predominant species after catalyst loading on ceria, it was decided to start here with a Pt(II) precursor, $PtCl_2(MeCN)_2$.

Early attempts at synthesis of catalyst used acetonitrile as the solvent (improved solubility of $PtCl_2(MeCN)_2$) for binding the ligand to the oxide surface, but the recyclability of the catalyst (Fig. S9) and Pt loading (Table S2) were much lower than for catalysts prepared in water. Two synthetic routes for SACs were explored to optimize catalyst activity. In the wet impregnation method reported by our group,[35] the ligand and ceria were allowed to stir for about 1.5 hours in water followed by addition of a metal precursor and stirring for 12 hours (Method 1). Alternatively, due to the poor solubility of $PtCl_2(MeCN)_2$ in water, the ligand and $PtCl_2(MeCN)_2$ were allowed to stir

for 12 hours in water before the introduction of ceria and stirring for an additional 12 hours (Method 2) in order to allow for Pt-Ligand complexation.

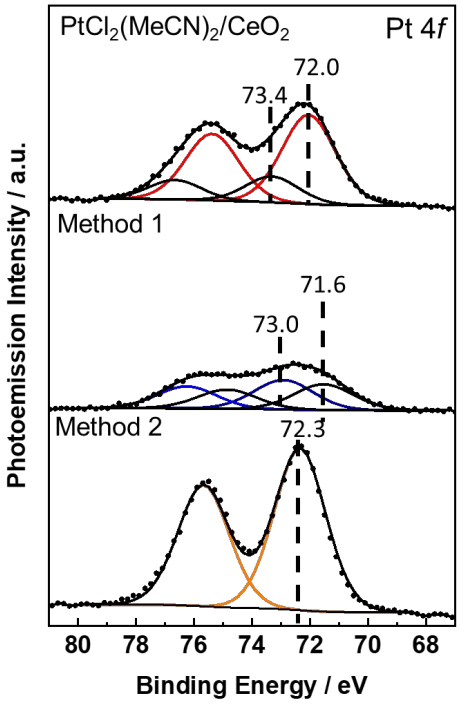

Fig. 2. Pt 4f XPS spectra of $PtCl_2(MeCN)_2/CeO_2$ (top), Pt-PDO/CeO_2 prepared by Method 1 (middle), Pt-PDO/CeO_2 prepared by Method 2 (bottom). Unless otherwise stated, all XPS spectra are normalized to the Ce 3d peak.

Pt 4f XPS spectra (Fig. 2) show that Method 2 resulted in a better control of the oxidation state of Pt on the surface because the Pt peaks are sharper and fit well by a single component pair (FWHM = 2.09 eV), while for Method 1, the data are much broader and require two fit component pairs (FWHM = 2.40 eV). This effect is strongest when PDO is used. Similar Pt(II) species are observed for PDO-C and PDO-C2 using both synthetic methods (Figs. S11-S12), suggesting that these ligands bind predominantly to the surface through carboxylic acid group followed by complexation of the Pt(II) precursor and are relatively unaffected by the order of addition to the solution. In contrast, the PDO ligand results in very different Pt(II) species being deposited on ceria for synthetic Methods 1 vs. 2. The Pt 4f XPS spectrum of ceria impregnated with $PtCl_2(MeCN)_2$ is fitted with two peaks (FWHM = 2.24 eV) whose binding energies do not match peaks for catalyst prepared using Methods 1 and 2 suggesting that a Pt-PDO complex forms on the surface of ceria.

Table 1. Comparison of XPS Element Ratios and Pt loading for different synthetic methods for freshly prepared catalysts and Pt loading for used catalysts: [a] 4 cycles, [b] 8 cycles. [c]STD is ± 0.01

Catalyst	***Cl:Pt***	***N:Pt***	***Pt:Ce***	***N:Ce***	***ICP/MS Pt (wt%) fresh[c]***	***ICP/MS Pt (wt%) used[c]***
$PtCl_2(MeCN)_2/CeO_2$	0.56	0.74	0.44	0.33	0.31	0.14[a]
Synthetic Method 1						
Pt-PDO/CeO_2	0.00	1.92	0.23	0.45	0.13	0.030[b]

Pt-PDO-C/CeO_2	0.54	4.92	0.38	1.88	0.37	0.11[b]
Pt-PDO-C2/CeO_2	0.00	25.6	0.047	1.20	0.021	0.021[a]
Synthetic Method 2						
Pt-PDO/CeO_2	0.75	1.30	0.68	0.88	0.55	0.056[b]
Pt-PDO-C/CeO_2	0.69	3.05	0.37	1.11	0.35	0.012[b]
Pt-PDO-C2/CeO_2	0.00	14.8	0.098	1.44	0.12	0.019[b]

For each of the Pt(II) catalysts, the Cl:Pt atom ratio measured by XPS (Table 1) is always less than 1, indicating that most of the chloride ligands from the Pt precursor are substituted with an incoming ligand or with surface hydroxy groups. This effect is strongest for Pt-PDO-C2 with either synthesis method and for Pt-PDO by Method 1, in which case there is no residual Cl detected by XPS. The N:Ce ratios (Table 1) indicate that the substituted ligands (PDO-C and PDO-C2) bind better to the surface than PDO using either synthesis method. This is consistent with N:Ce ratios for Ligand/CeO_2 (Table S3) showing higher ligand loading for ligands containing carboxylic acid groups than PDO. When no metal is present, higher loading for PDO-C and PDO-C2 is likely due to a direct ligand-support interaction rather than a metal-mediated interaction. The N 1s spectrum of Ligand/CeO_2 versus Pt-Ligand/CeO_2 (Fig. S17) show that the FWHM (1.63 vs 1.72 eV) for PDO-C2 is similar, whereas the FWHM is larger for Pt-PDO/CeO_2 (2.44 vs 3.00 eV) and Pt-PDO-C/CeO_2 (1.83 vs 2.50 eV). This is consistent with PDO and PDO-C showing higher metal loading than PDO-C2. This implies that the ceria surface of Pt-PDO-C2/CeO_2 is predominantly covered with PDO-C2 and very low concentration of metal.

The PDO-C2 ligand gives the lowest Pt loading of ligands reported in this study and may be attributed to increased steric hindrance, and binding of both carboxylic acid groups to the surface may interfere with the coordination of platinum. The lower steric profile of PDO (Fig. S18) compared to the substituted PDO ligands may explain a higher metal loading for PDO using synthetic method 2. The platinum loading and Pt 4f XPS spectra of freshly prepared catalysts using PDO-C and PDO-C2 ligands are similar using both synthetic methods. This suggests that the substituted PDO ligands are depositing on the surface, which is followed by binding of the metal. We explored complexation of the ligand with $PtCl_2(MeCN)_2$ by ^1H NMR in the absence of ceria in DMSO-d_6 and demonstrated that, of the three ligands studied, only PDO coordinates in solution (Fig. S19).

DRIFT spectra for Pt(II)-Ligand/CeO_2 with each ligand prepared using Method 2 (Fig. 3) show that the preferred site for binding catalyst to surface is the terminal hydroxy site.[43, 44] Peaks appearing from 3000-3100 cm^{-1} indicate aromatic C-H groups and ketone stretches at 1744-1708 cm^{-1} additionally confirm that PDO-C and PDO-C2 are on surface. The intensity of the ketone stretch for PDO-C (1709 cm^{-1}) and PDO-C2 (1704 cm^{-1}) is higher than for PDO (1706 cm^{-1}), consistent with higher ligand loading on surface for PDO ligands containing anchoring groups evaluated via XPS (Table 1 and S3, and Fig. S17).

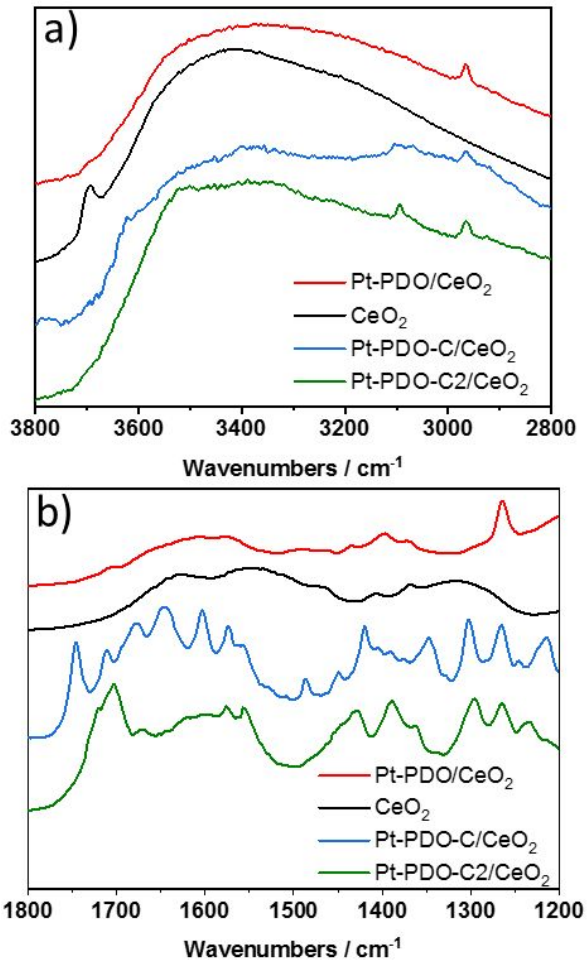

Fig. 3. DRIFTS spectra for CeO_2 (black), Pt-PDO/CeO_2 (red), Pt-PDO-C/CeO_2 (blue), and Pt-PDO-C2/CeO_2 (green).

Systematic studies of ligands on ceria demonstrate that the incorporation of COOH groups into PDO results in the complete disappearance of the terminal hydroxy group (3700 cm^{-1}), whereas the hydroxy peak remains using an equimolar loading of PDO (Fig. S24). This shows that the reaction of carboxylic acid groups with the terminal ceria hydroxy groups is more favorable than hydrogen bonding with PDO using a similar concentration of ligand exposed to ceria. Control reactions of both trimesic acid and 4-fluorobenzoic acid with ceria under similar reaction conditions result in a high degree of surface bonding. This further demonstrates that carboxylic acid groups can chemisorb onto ceria surfaces at terminal hydroxy sites on ceria (Fig. S29), supporting our hypothesis that the carboxylic acid groups anchor our ligands to the surface.

The implication of collective XPS and DRIFTS data is that for the ligands PDO-C and PDO-C2 the carboxylic acid reacts with terminal surface hydroxy sites to anchor the ligand to surface. The ligand on ceria can then coordinate $PtCl_2(MeCN)_2$ that can lose n HCl, where n = 1 or 2, through a reaction with surface hydroxy groups or proton responsive functional groups on substituted PDO ligands (Scheme 4). The preliminary formation of a Pt-PDO complex in solution may also deposit on ceria, especially using synthetic Method 2. One explanation for the differences

observed between Method 1 and 2 is that hydrogen bonding of PDO with surface hydroxy sites before addition of the Pt(II) precursor may prevent deposition and coordination of $PtCl_2(MeCN)_2$ on ceria or assist in the removal of HCl as [HPDO][Cl] using synthetic Method 1.

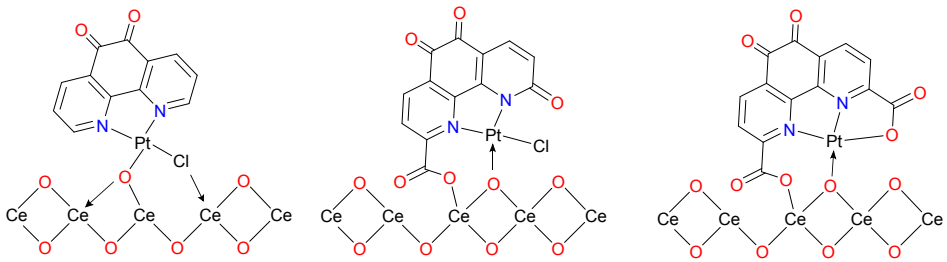

Scheme 4. Proposed Pt-PDO, Pt-PDO-C, and Pt-PDO-C2 species on CeO_2 surface.

Using extended x-ray absorption fine structure (EXAFS) spectroscopy at the Pt L_3-edge, the Pt-PDO catalyst was examined before and after reaction for the presence of Pt-Pt bonds and changes in the Pt coordination environment that could contribute to changes in activity of the catalyst (Fig. S30). The Pt-PDO samples do not show any Pt-Pt scattering before or after reaction, indicating that there is not significant Pt sintering in this system (Table S4). However, there is a notable loss of Cl after the reaction (Table S4). CO adsorption experiments confirm single atom character and also demonstrate the loss of Cl at elevated temperature (Fig. S54). Each of these results is consistent with prior studies from our lab.[36] In the case of the Pt-PDO-C sample, we do observe Pt-Pt scattering after reaction, indicating that there may be some aggregation of Pt in this sample during catalysis.

3.3 Recyclability of Ceria supported Pt catalysts

Recyclability tests of Pt-Ligand/CeO_2 SACs, where Ligand = PDO and PDO-C, prepared by methods 1 and 2 gave similar recyclability (Fig. 4) where the hydrosilylation yield gradually decreased with successive batch cycles. The data displayed for PDO are an average of three runs and for PDO-C an average of two runs.

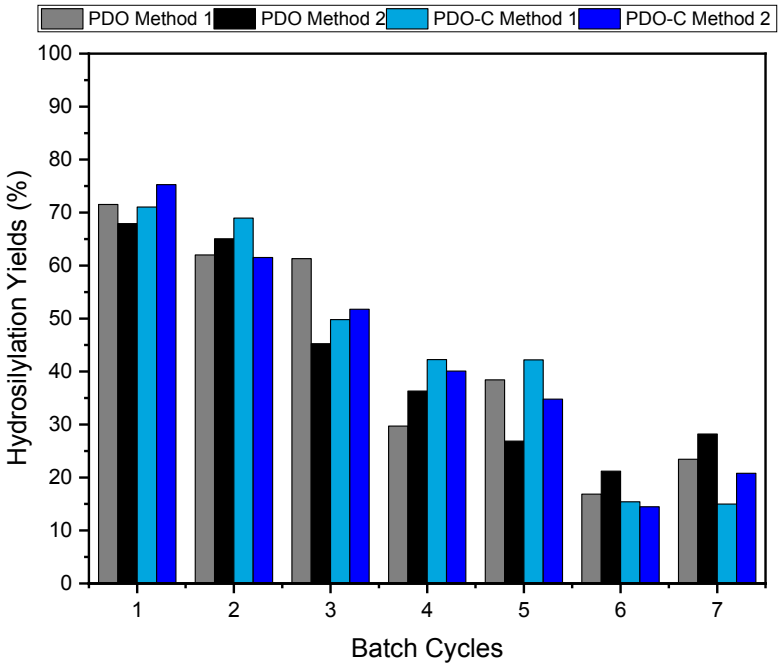

Fig. 4. Comparison of hydrosilylation yields for seven consecutive runs using Pt-Ligand/CeO_2, where L = PDO (gray and black) and PDO-C (light blue and blue) prepared by synthetic methods 1 and 2. PDO-C2 showed little to no reactivity (Fig. S32).

Incorporating one carboxylic acid group in the PDO ligand does not improve the yield compared to PDO, but the turnover number is higher for Pt-PDO-C/CeO_2 (7381) than for Pt-PDO/CeO_2 (4000), prepared using Method 2. This indicates that the lower metal loading for Pt-PDO-C/CeO_2 (1st batch) was more active for hydrosilylation. Platinum loading before and after catalysis is comparable for PDO-C using both synthetic methods, whereas higher metal loading for PDO ligand in Method 2 did not show improved hydrosilylation yield. The selectivity is the same for all catalysts; only the anti-Markovnikov product (**1**) and the rearranged silylated product (**3**) are observed by GC/MS (Fig. S33).

The PDO-C2 ligand gives the worst performance (Fig. S32), attributed to a combination of low metal loading and the presence of two COOH groups near the binding pocket that would afford a saturated metal complex which impairs olefin coordination. This seems reasonable since a crystal structure (Fig. S8) was obtained that shows the connectivity of PDO-C with Pt(II) that would imply that the carboxylic acid groups are too close to the binding pocket and can coordinate to platinum instead of at the ceria surface.

3.4 Understanding Deactivation of Pt SACs

The DRIFTS spectrum was collected on Pt-PDO/CeO_2 (prepared using Method 2) after 8 cycles of hydrosilylation and compared to the spectrum before catalysis (Fig. 5). Very intense peaks appearing at 2165 cm^{-1} (Si-H stretch), 1127-1047 cm^{-1} (Si-O and Si-O-Si), and 1272 and 910 cm^{-1} (CH_3 of siloxanes) indicate silane is depositing on the surface. Decrease, following catalysis, in XPS peak intensities for Ce 3d, Pt 4f, N1s, and Cl 2p spectra (Fig. S34-S35) and an appearance of new peaks in the Si 2p and O 1s XPS spectra (Fig. 6) provide independent evidence of coverage of the surface by silane. Similar changes are observed in XPS and DRIFTS spectra for Pt/Ligand/CeO_2, where Ligand is PDO-C and PDO-C2, after several cycles (Fig. S38-S43).

Fig. 5. DRIFTS spectra for Pt-PDO/CeO_2 before (black) and after catalysis 8 cycles (red).

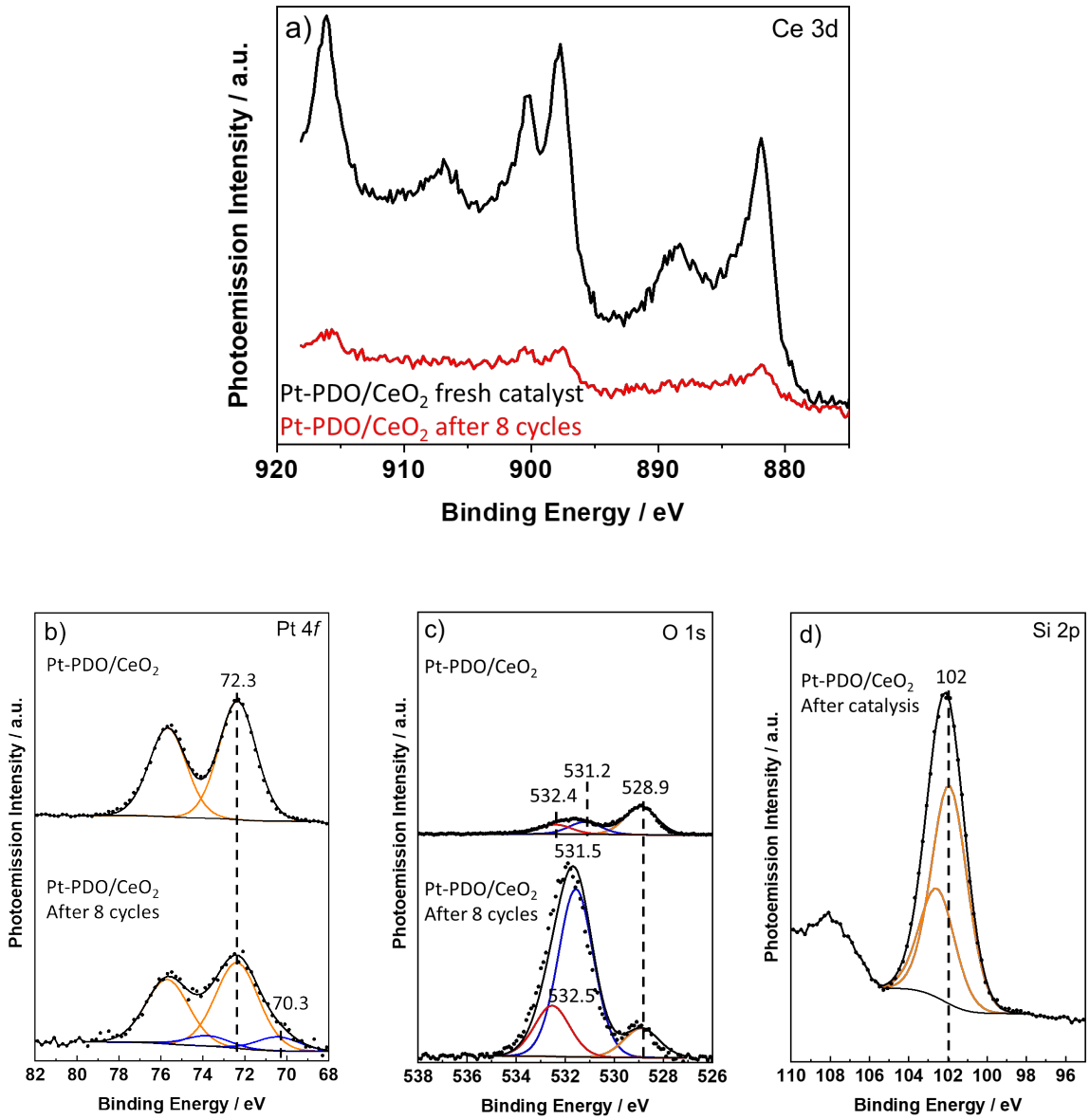

Fig. 6. a) Ce 3d XPS spectra of Pt-PDO/CeO_2 before (FWHM = 2.09) (black) and after 8 cycles of hydrosilylation (FWHM = 2.47) (red). Stacked Pt 4f (b) and O 1s (c) XPS spectra of Pt-PDO/CeO_2 before (top) and after 8 cycles of hydrosilylation (bottom) and Si 2p (d) XPS spectra of Pt-PDO/CeO_2 after 8 cycles of hydrosilylation.

The Pt 4f spectrum after 8 cycles of catalysis (Fig. 6, a) shows a decrease in peak intensity for the Pt(II) species at 72.3 eV, consistent with a decrease in the Pt concentration observed by ICP/MS. The formation of a lower valent Pt species at 70.3 eV could be attributed to the reducing conditions imparted by the silane reagent. In addition to metal leaching and nanoparticle formation, silane buildup could therefore explain the decrease in catalytic activity.

3.5 Investigation of Silane Reactions with Ceria

For comparison to the above, we studied a control reaction of simply H-Si(OMe)$_2$Me + CeO_2 in toluene at 70 °C for 20 minutes and observed a Si-H stretch in DRIFTS and Si 2p peak in XPS spectrum. The DRIFTS spectrum shows a strong peak at 2165 cm^{-1} indicating Si-H on the surface (Figure 7). The presence of peaks at 1117 and 1047 cm^{-1} are consistent with Si-O and Si-O-Si bond stretches, and the peak at 910, 1271, and 2968 cm^{-1} is characteristic of CH_3.[45] The disappearance of the terminal hydroxy peak at 3700 cm^{-1} [43, 44] is consistent with silicon replacing hydroxy protons. Reported literature on ceria reactivity with silanes shows that terminal hydroxy groups can react with siloxy groups to release alcohol and form Ce-O-SiR_3 moieties.[46, 47] The several proposed silanes chemisorbed on the surface, consistent with these observations, are shown in Scheme 5.

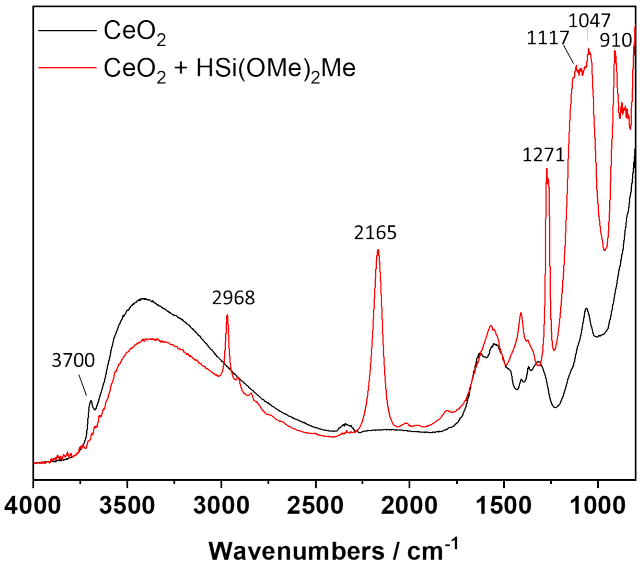

Fig. 7. DRIFTS spectra of CeO_2 (black) and CeO_2 + HSi(OMe)$_2$Me in toluene at 70 °C for 20 minutes (red).

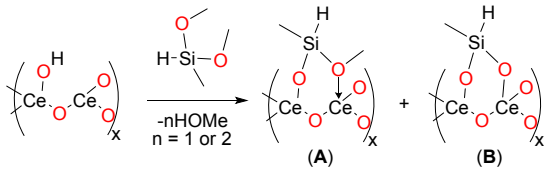

Scheme 5. Proposed silane species from reaction of ceria and silane.

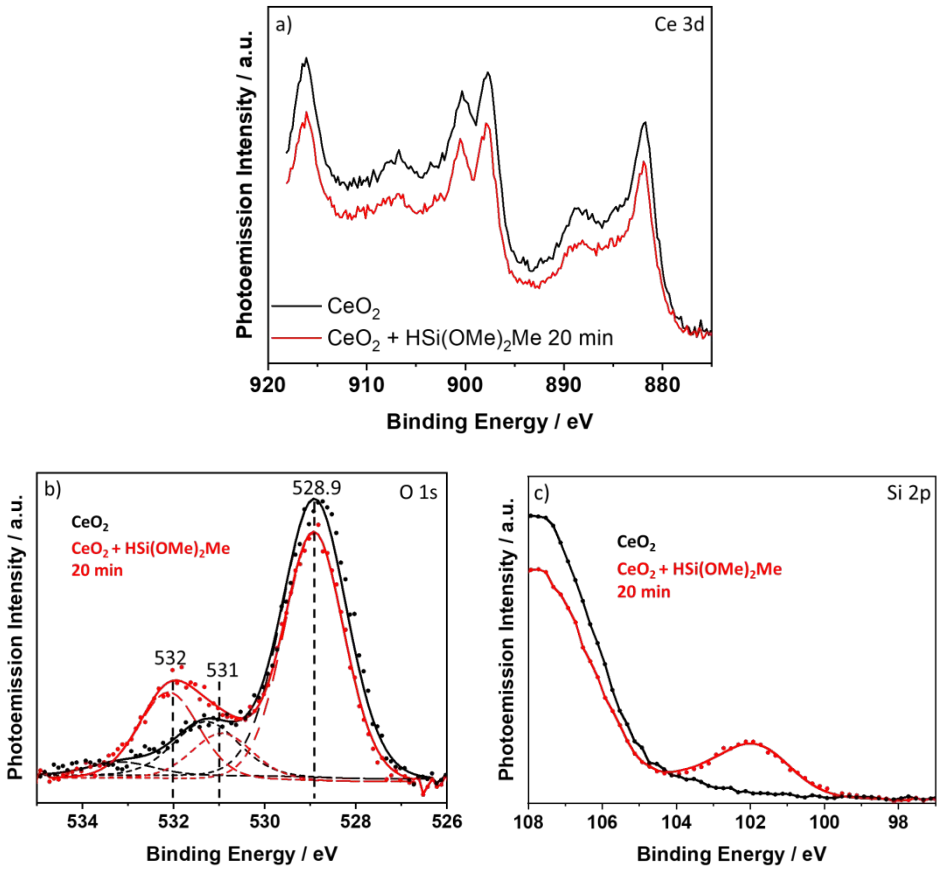

Fig. 8. Ce 3d (a), O 1s (b), and Si 2p (c) XPS spectra for CeO_2 (black) and CeO_2 exposed to $HSi(OMe)_2Me$ for 20 minutes at 70 °C in toluene (red).

The intensity of Ce 3d peaks in the XPS spectrum shows a decrease after additional heating. We interpret this as covering of ceria by an overlayer of silane reagent. Based on the Ce 3d attenuation of 19%, we estimate the silane coverage to have a thickness of approximately 1.5 – 2.2 nm (Eqn. S1).[48,49, 50] The O 1s peak at 528.9 eV, corresponding to lattice oxygen,[51] has reduced intensity after exposure to $HSi(OMe)_2Me$, again consistent with overlayer coverage. The O 1s peak at 531.3 eV, assigned as surface hydroxy oxygen,[51, 52] is overwhelmed by the appearance of a new peak at 531.9 eV and assumed to no longer contribute to this signal due to absence of hydroxy groups (DRIFTS evidence). This peak at 531.9 eV (FWHM = 2.18 eV) is wider than the peak at 528.9 eV (FWHM = 1.55 eV), justifying a fit with two components at 531.0 and 532.0 eV (both FWHM 1.55 eV). The peak at 531.0 eV is assigned to Si-O-Si and the peak at 532.0 eV is assigned to Si-O-Ce. The ratio of O 1s peak area at 532.0 eV and 531.0 eV is roughly 2:1, which suggests that we have mixture of components **A** and **B** (Scheme 5). The C 1s spectrum (Fig. S44) shows an increase of peak intensity at 284.4 eV, which is consistent with a buildup of sp^3 carbon on the surface. The Si 2p spectrum shows a peak at 101.7 eV whose binding energy is consistent with siloxanes that contain $Si\text{-}CH_3$ and Si-O linkages.[53] Note that we do not have an

indication of a different product distribution (A vs. B in Scheme 5), but the surface binding may favor certain products for adsorption.

The above data shows that $HSi(OMe)_2Me$ reacts with ceria, in addition to platinum sites, and this competing reaction can explain why a higher loading of $HSi(OMe)_2Me$ has been observed to give higher hydrosilylation yields. Heating $HSi(OMe)_2Me$ with ceria in toluene for 2 hours shows an increase in silicon and oxygen peaks compared to heating for 20 minutes demonstrating that silane accumulates on the surface with successive runs (Fig. S45-S46). XPS and DRIFTS data demonstrated that silicon *deposits progressively* on the surface with repeated runs and leads to a decrease in signal intensity observed in Ce 3d, Pt 4f, and N 1s XPS spectra. The buildup of silane on the surface alone is not the sole cause of lowered catalyst activity, because the samples that showed an absence of peaks in the Pt 4f XPS spectra (Fig. S10, Table S2) have been shown to contain Pt by ICP/MS, but the Pt loading for these samples was much lower than the values for freshly prepared catalyst.

An extensive study of silanes containing OMe, Cl, and phenyl substituents (Fig. S47-S53) has shown that, under our reaction conditions, these all add silyl groups to ceria, replacing ceria hydroxyl groups. This confirms the above assignments of DRIFTS and XPS signatures, including the decreased Ce 3d XPS intensity following silylation. These Si-heteroatom bonds are the cause of surface silylation.

4. Conclusion

We have shown that the incorporation of carboxylic acid groups in PDO result in higher ligand loading for PDO-C and PDO-C2 than the unsubstituted diimine PDO on ceria. Exploration of a new impregnation method demonstrates that preliminary complexation of Pt(II) by PDO (Method 2) leads to a more uniform Pt oxidation state than ligand loading on ceria first (Method 1). For PDO-C and PDO-C2, similar results in Pt 4f XPS data are interpreted to indicate that the carboxylic acid binds to the surface first, followed by metal complexation. Terminal hydroxy groups on the ceria react with carboxylic acids to chemisorb PDO-C and PDO-C2 to the surface, representing sites for metal complex deposition.

Hydrosilylation yields with $HSi(OMe)_2Me$ were comparable for PDO and PDO-C. The ligand PDO-C2 containing two carboxylic acid groups ortho to nitrogen resulted in SACs with lower metal loading, lower recyclability, and lower activity than PDO. A crystal structure of Pt complexed to PDO-C shows that the carboxylic acid group can coordinate to the metal, and for PDO-C2, the incorporation of two $–CO_2H$ groups ortho to the nitrogen atoms may suppress catalytic activity due to a saturated Pt center. In addition, high N:Ce ratios and lowest platinum loading suggest that the binding of PDO-C2 to the surface may inhibit metal uptake, explaining low catalytic activity for PDO-C2. Future designs should incorporate carboxylic acid groups further away from the binding pocket of the ligand.

For all Pt-Ligand/CeO_2 catalysts studied, the XPS and DRIFTS data showed that, after several cycles of catalysis, new Si and O species appear indicating accumulation of silane reagent on the ceria surface. Pt 4f XPS spectra before and after catalysis show that the Pt(II) oxidation state did not change but peak intensity decreased, consistent with decreased exposure of Pt. EXAFS

measurements agree with a chloride loss observed in XPS. Pt L_3-edge EXAFS shows formation of Pt-Pt bonds on the surface, suggesting that nanoparticle formation may be contributing to catalyst degradation in case of PDO-C ligand. Both catalyst leaching, as shown by loss of total Pt by ICP/MS, and silane buildup explain reduced hydrosilylation yields after successive cycles. Silanes $HSiR_3$ (R = hydrocarbyl) are thus recommended for improved hydrosilylation SACs, based on these results with $HSi(OMe)_2Me$; the methoxy group on silicon is thus a vulnerability in hydrosilylation with any metal oxide support.

Accession Code

CCDC 2171923 contains the supplementary crystallographic data for this paper. These data can be obtained free of charge via www.ccdc.cam.ac.uk/data_request/cif, or by emailing data_request@ccdc.cam.ac.uk, or by contacting The Cambridge Crystallographic Data Centre, 12 Union Road, Cambridge CB2 1EZ, UK; fax: +44 1223 336033.

Acknowledgement

This work was supported by the U. S. Department of Energy, Office of Basic Energy Sciences, Chemical Sciences program, DE-SC0021390. XPS measurements were carried out at the Indiana University (IU) Nanoscale Characterization Facility, with assistance from Dr. Yaroslav Lasovyj. EXAFS measurements were performed at beamline 9-BM at the Advanced Photon Source, an Office of Science User Facility operated for the U.S. Department of Energy (DOE) Office of Science by Argonne National Laboratory, under Contract No. DE-AC02-06CH11357. Support for the acquisition of the Bruker Venture D8 diffractometer through the Major Scientific Research Equipment Fund from the President of Indiana University and the Office of the Vice President for Research is gratefully acknowledged. We thank Ms. Ayanna Culmer-Gilbert for assistance with synthesis of some catalysts. Catalysts were analyzed utilizing an Agilent 7700 ICP-MS within the Metal Isotopes Laboratory at Indiana University by Dr. Shelby Rader. GC-MS measurements were conducted in the IU Mass Spectrometry Facility with assistance from Dr. Angie Hansen and Dr. Robert H. Pepin.

1. Maciejewski, H.; Wawrzyńczak, A.; Dutkiewicz, M.; Fiedorow, R., Silicone waxes—synthesis via hydrosilylation in homo- and heterogeneous systems. *J. Mol. Catal. A: Chem.* **2006,** *257* (1), 141-148.
2. Pierce, O. R.; Kim, Y. K., Fluorosilicones as High Temperature Elastomers. *Rubber Chem. Technol.* **1971,** *44* (5), 1350-1362.
3. Morita, Y.; Tajima, S.; Suzuki, H.; Sugino, H., Thermally initiated cationic polymerization and properties of epoxy siloxane. *J. Appl. Polym. Sci.* **2006,** *100* (3), 2010-2019.
4. Beyou, E.; Babin, P.; Bennetau, B.; Dunogues, J.; Teyssie, D.; Boileau, S., New fluorinated polysiloxanes containing an ester function in the spacer. I. Synthesis and characterization. *J. Polym. Sci., Part A: Polym. Chem.* **1994,** *32* (9), 1673-1681.
5. Iojoiu, C.; Abadie, M. J. M.; Harabagiu, V.; Pinteala, M.; Simionescu, B. C., Synthesis and photocrosslinking of benzyl acrylate substituted polydimethylsiloxanes. *Eur. Polym. J.* **2000,** *36* (10), 2115-2123.

6. Li, Z.; Qin, J.; Yang, Z.; Ye, C., Synthesis and structural characterization of a new polysiloxane with second-order nonlinear optical effect. *J. Appl. Polym. Sci.* **2004,** *94* (2), 769-774.
7. Drazkowski, D. B.; Lee, A.; Haddad, T. S.; Cookson, D. J., Chemical Substituent Effects on Morphological Transitions in Styrene−Butadiene−Styrene Triblock Copolymer Grafted with Polyhedral Oligomeric Silsesquioxanes. *Macromolecules* **2006,** *39* (5), 1854-1863.
8. Tuchbreiter, A.; Werner, H.; Gade, L. H., "A posteriori" modification of carbosilane dendrimers and dendrons: their activation in core and branch positions. *Dalton Trans.* **2005,** (8), 1394-1402.
9. Troegel, D.; Stohrer, J., Recent advances and actual challenges in late transition metal catalyzed hydrosilylation of olefins from an industrial point of view. *Coord. Chem. Rev.* **2011,** *255* (13), 1440-1459.
10. Marciniec, B. In *Hydrosilylation : a comprehensive review on recent advances*, 2010.
11. Ganicz, T.; Pakuła, T.; Stańczyk, W. A., Novel liquid crystalline resins based on MQ siloxanes. *J. Organomet. Chem.* **2006,** *691* (23), 5052-5055.
12. Speier, J. L.; Webster, J. A.; Barnes, G. H., The Addition of Silicon Hydrides to Olefinic Double Bonds. Part II. The Use of Group VIII Metal Catalysts. *J. Am. Chem. Soc.* **1957,** *79* (4), 974-979.
13. Karstedt, B., **1973**.
14. Karstedt, B., Platinum complexes of unsaturated siloxanes and platinum containing organopolysiloxanes. US Patent 3,775,452: 1973.
15. Xue, M.; Li, J.; Peng, J.; Bai, Y.; Zhang, G.; Xiao, W.; Lai, G., Effect of triarylphosphane ligands on the rhodium-catalyzed hydrosilylation of alkene. *Appl. Organomet. Chem.* **2014,** *28* (2), 120-126.
16. Igarashi, M.; Matsumoto, T.; Kobayashi, T.; Sato, K.; Ando, W.; Shimada, S.; Hara, M.; Uchida, H., Ir-catalyzed hydrosilylation reaction of allyl acetate with octakis (dimethylsiloxy) octasilsesquioxane and related hydrosilanes. *J. Organomet. Chem.* **2014,** *752*, 141-146.
17. Dong, H.; Jiang, Y.; Berke, H., Rhenium-mediated dehydrogenative silylation and highly regioselective hydrosilylation of nitrile substituted olefins. *J. Organomet. Chem.* **2014,** *750*, 17-22.
18. Wu, J. Y.; Stanzl, B. N.; Ritter, T., A strategy for the synthesis of well-defined iron catalysts and application to regioselective diene hydrosilylation. *J. Am. Chem. Soc.* **2010,** *132* (38), 13214-13216.
19. Glaser, P. B.; Tilley, T. D., Catalytic hydrosilylation of alkenes by a ruthenium silylene complex. Evidence for a new hydrosilylation mechanism. *J. Am. Chem. Soc.* **2003,** *125* (45), 13640-13641.
20. Nozakura, S.; Konotsune, S., Cyanoethylation of Trichlorosilane. II. α-Addition. *Bull. Chem. Soc. Jpn.* **1956,** *29* (3), 326-331.
21. Bareille, L.; Becht, S.; Cui, J. L.; Le Gendre, P.; Moïse, C., First Titanium-Catalyzed a nti-1, 4-Hydrosilylation of Dienes. *Organometallics* **2005,** *24* (24), 5802-5806.
22. Harder, S.; Brettar, J., Rational Design of a Well-Defined Soluble Calcium Hydride Complex. *Angew. Chem. Int. Ed.* **2006,** *45* (21), 3474-3478.
23. Leich, V.; Spaniol, T. P.; Maron, L.; Okuda, J., Hydrosilylation catalysis by an earth alkaline metal silyl: synthesis, characterization, and reactivity of bis (triphenylsilyl) calcium. *Chem. Commun.* **2014,** *50* (18), 2311-2314.
24. Zhu, Y.; Cao, T.; Cao, C.; Luo, J.; Chen, W.; Zheng, L.; Dong, J.; Zhang, J.; Han, Y.; Li, Z.; Chen, C.; Peng, Q.; Wang, D.; Li, Y., One-Pot Pyrolysis to N-Doped Graphene with High-Density Pt Single Atomic Sites as Heterogeneous Catalyst for Alkene Hydrosilylation. *ACS Catal.* **2018,** *8* (11), 10004-10011.
25. Chen, Y.; Ji, S.; Sun, W.; Chen, W.; Dong, J.; Wen, J.; Zhang, J.; Li, Z.; Zheng, L.; Chen, C.; Peng, Q.; Wang, D.; Li, Y., Discovering Partially Charged Single-Atom Pt for Enhanced Anti-Markovnikov Alkene Hydrosilylation. *J. Am. Chem. Soc.* **2018,** *140* (24), 7407-7410.
26. Galeandro-Diamant, T.; Zanota, M.-L.; Sayah, R.; Veyre, L.; Nikitine, C.; de Bellefon, C.; Marrot, S.; Meille, V.; Thieuleux, C., Platinum nanoparticles in suspension are as efficient as Karstedt's complex for alkene hydrosilylation. *Chem. Commun.* **2015,** *51* (90), 16194-16196.

27. Chauhan, B. P.; Rathore, J. S., Regioselective Synthesis of Multifunctional Hybrid Polysiloxanes Achieved by Pt−Nanocluster Catalysis. *J. Am. Chem. Soc.* **2005,** *127* (16), 5790-5791.
28. Bai, Y.; Zhang, S.; Deng, Y.; Peng, J.; Li, J.; Hu, Y.; Li, X.; Lai, G., Use of functionalized PEG with 4-aminobenzoic acid stabilized platinum nanoparticles as an efficient catalyst for the hydrosilylation of alkenes. *J. Colloid Interface Sci.* **2013,** *394*, 428-433.
29. Stein, J.; Lewis, L.; Gao, Y.; Scott, R., In situ determination of the active catalyst in hydrosilylation reactions using highly reactive Pt (0) catalyst precursors. *J. Am. Chem. Soc.* **1999,** *121* (15), 3693-3703.
30. Meister, T. K.; Riener, K.; Gigler, P.; Stohrer, J. r.; Herrmann, W. A.; Kühn, F. E., Platinum Catalysis Revisited - Unraveling Principles of Catalytic Olefin Hydrosilylation. *ACS Catal.* **2016,** *6* (2), 1274-1284.
31. Chen, L.; Ali, I. S.; Sterbinsky, G. E.; Gamler, J. T. L.; Skrabalak, S. E.; Tait, S. L., Alkene Hydrosilylation on Oxide-Supported Pt-Ligand Single-Site Catalysts. *ChemCatChem* **2019,** *11* (12), 2843-2854.
32. Zhou, X.; Chen, L.; Sterbinsky, G. E.; Mukherjee, D.; Unocic, R. R.; Tait, S. L., Pt-Ligand single-atom catalysts: tuning activity by oxide support defect density. *Catal. Sci. Technol.* **2020,** *10* (10), 3353-3365.
33. Cui, X.; Junge, K.; Dai, X.; Kreyenschulte, C.; Pohl, M.-M.; Wohlrab, S.; Shi, F.; Brückner, A.; Beller, M., Synthesis of Single Atom Based Heterogeneous Platinum Catalysts: High Selectivity and Activity for Hydrosilylation Reactions. *ACS Cent. Sci.* **2017,** *3* (6), 580-585.
34. Guo, P.; Liu, H.; Zhao, J., Transforming bulk alkenes and alkynes into fine chemicals enabled by single-atom site catalysis. *Nano Research* **2022**.
35. Chen, L.; Ali, I. S.; Tait, S. L., Bidentate N-based Ligands for Highly Reusable, Ligand-coordinated, Supported Pt Hydrosilylation Catalysts. *ChemCatChem* **2020,** *12* (13), 3576-3584.
36. Zhou, X.; Sterbinsky, G. E.; Wasim, E.; Chen, L.; Tait, S. L., Tuning Ligand-Coordinated Single Metal Atoms on TiO2 and their Dynamic Response during Hydrogenation Catalysis. *ChemSusChem* **2021,** *14* (18), 3825-3837.
37. Jin, S.; Wen, M.-F.; Liu, L.-F.; Gao, M.-J.; Wu, J.-Z., Synthesis and supramolecular networks of 5,6-dioxo-1,10-phenanthroline-2,9-dicarboxylic acid dihydrate and its first coordination compound cis-diaquachlorido(5,6-dioxo-1,10-phenanthroline-2,9-dicarboxylic acid-κ4O2,N,N′,O9)manganese(II) chloride dihydrate. *Acta Crystallogr. Sect. C: Cryst. Struct. Commun.* **2012,** *68* (5), m135-m138.
38. Xiao, C.-L.; Wang, C.-Z.; Yuan, L.-Y.; Li, B.; He, H.; Wang, S.; Zhao, Y.-L.; Chai, Z.-F.; Shi, W.-Q., Excellent Selectivity for Actinides with a Tetradentate 2,9-Diamide-1,10-Phenanthroline Ligand in Highly Acidic Solution: A Hard–Soft Donor Combined Strategy. *Inorg. Chem.* **2014,** *53* (3), 1712-1720.
39. Chandler, C. J.; Deady, L. W.; Reiss, J. A., Synthesis of some 2,9-disubstituted-1,10-phenanthrolines. *J. Heterocycl. Chem.* **1981,** *18* (3), 599-601.
40. Fraccarollo, D.; Bertani, R.; Mozzon, M.; Belluco, U.; Michelin, R. A., Synthesis and spectroscopic investigation of cis and trans isomers of bis(nitrile)dichloroplatinum(II) complexes. *Inorg. Chim. Acta* **1992,** *201* (1), 15-22.
41. Kochi, J. K., Formation of Alkyl Halides from Acids by Decarboxylation with Lead(IV) Acetate and Halide Salts. *J. Org. Chem.* **1965,** *30* (10), 3265-3271.
42. Kochi, J. K.; Bemis, A.; Jenkins, C. L., Mechanism of electron transfer oxidation of alkyl radicals by copper(II) complexes. *J. Am. Chem. Soc.* **1968,** *90* (17), 4616-4625.
43. Badri, A.; Binet, C.; Lavalley, J.-C., An FTIR study of surface ceria hydroxy groups during a redox process with H2. *J. Chem. Soc., Faraday Trans.* **1996,** *92* (23), 4669-4673.
44. Hadjiivanov, K., Identification and Characterization of Surface Hydroxyl Groups by Infrared Spectroscopy. *Advances in Catalysis* **2014,** *57*, 99-318.

45. DeRita, L.; Dai, S.; Lopez-Zepeda, K.; Pham, N.; Graham, G. W.; Pan, X.; Christopher, P., Catalyst architecture for stable single atom dispersion enables site-specific spectroscopic and reactivity measurements of CO adsorbed to Pt atoms, oxidized Pt clusters, and metallic Pt clusters on TiO2. *Journal of the American Chemical Society* **2017,** *139* (40), 14150-14165.
46. Hepburn, C. A.; Vale, P.; Brown, A. S.; Simms, N. J.; McAdam, E. J., Development of on-line FTIR spectroscopy for siloxane detection in biogas to enhance carbon contactor management. *Talanta* **2015,** *141*, 128-136.
47. Pleul, D.; Frenzel, R.; Eschner, M.; Simon, F., X-ray photoelectron spectroscopy for detection of the different Si–O bonding states of silicon. *Anal. Bioanal. Chem.* **2003,** *375* (8), 1276-1281.
48. Ma, H.; Ren, H.; Koshy, P.; Sorrell, C. C.; Hart, J. N., Enhancement of CeO2 Silanization by Spontaneous Breakage of Si–O Bonds through Facet Engineering. *J. Phys. Chem. C* **2020,** *124* (4), 2644-2655.
49. Estimate based on electron kinetic enegy of 586 eV and electron inelastic mean free path of 10-15 nm. Electron take-off angle is 45 degrees.
50. Ratner, B. D.; Castner, D. G., Electron Spectroscopy for Chemical Analysis. In *Surface Analysis - The Principal Techniques*, 2nd ed.; Vickerman, J. C.; Gilmore, I. S., Eds. John Wiley & Sons, Ltd.: 2009; pp 63-67.
51. Alford, T. L., Fundamentals of Nanoscale Film Analysis. Feldman, L. C.; Mayer, J. W., Eds. Springer Science+Business Media, Inc.: Boston, MA :, 2007; pp 106-109.
52. Natile, M. M.; Boccaletti, G.; Glisenti, A., Properties and Reactivity of Nanostructured CeO2 Powders: Comparison among Two Synthesis Procedures. *Chem. Mater.* **2005,** *17* (25), 6272-6286.
53. Mullins, D. R., The surface chemistry of cerium oxide. *Surf. Sci. Rep.* **2015,** *70* (1), 42-85.
54. Louette, P.; Bodino, F.; Pireaux, J.-J., Poly(dimethyl siloxane) (PDMS) XPS Reference Core Level and Energy Loss Spectra. *Surf. Sci. Spectra* **2005,** *12* (1), 38-43.